ACS Sustainable Chemistry & Engineering

Research Article

pubs.acs.org/journal/ascecg

Robust Wide Visible-Light-Responsive Photoactivity for H_2 Production over a Polymer/Polymer Heterojunction Photocatalyst: The Significance of Sacrificial Reagent

Xiaohu Zhang, Bosi Peng, Shuai Zhang, and Tianyou Peng*

College of Chemistry and Molecular Science, Wuhan University, Wuhan 430072, People's Republic of China

Supporting Information

ABSTRACT: A robust polymer/polymer surface heterojunction (SHJ) catalyst for wide visible-light-driven H_2 production is fabricated by a facile rotary evaporation of poly(3-hexylthiophene) (P3HT) solution containing graphitic carbon nitride (g-C_3N_4). The photocatalytic H_2 production activity of the obtained SHJ catalyst (P3HT/g-C_3N_4) is significantly affected by the types of sacrificial reagents, and ascorbic acid (AA) shows the best photoactivity among the commonly used sacrificial reagents. The SHJ catalyst containing 3 wt % P3HT gives a H_2 evolution activity up to 3045 μmol/h in a saturated AA solution, which is ~491 times higher than that (6.2 μmol/h) of P3HT/g-C_3N_4 without AA solution under $\lambda \geq 500$ nm light irradiation. Especially, the SHJ catalyst containing 3 wt % P3HT shows a record apparent quantum yield (AQY) of 77.4% at 420 nm light irradiation in the field of g-C_3N_4-based catalyst, and wide visible/NIR-light-responsive ability with AQY of 59.4%, 20.2%, 3.2% and 0.68% at 500, 600, 700 and 800 nm monochromatic light irradiation, respectively. The extremely high photoactivity is caused by the wide visible-light absorption, efficient charge transfer at the interface of P3HT/g-C_3N_4 and suitable oxidation half-reaction caused by the added AA as a sacrificial reagent. This study not only demonstrates a new direction for the solar fuel conversion over the large family of polymer-based semiconductors but also emphasizes the importance of oxidation half-reaction caused by the sacrificial reagent, which can significantly affect the photoactivity for H_2 production.

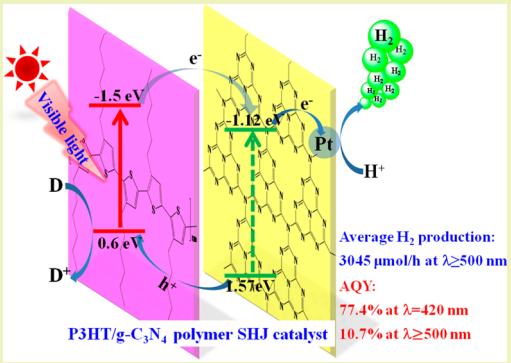

KEYWORDS: *Polymer/polymer heterojunction catalyst, Robust photoactivity, Hydrogen production, Wide visible-light response, Sacrificial reagent*

INTRODUCTION

To solve the current energy crisis, the development of economical, stable and highly effective sunlight-to-chemical fuel/electricity conversion systems, such as semiconductor-based photocatalytic H_2 production,[1−9] dye-sensitized solar cells[10] and polymer bulk heterojunction (BHJ) solar cells,[11−14] has drawn increasing attention. Among which, the BHJ solar cells based on the conjugated polymers acting as electron donors exhibit some advantages such as flexibility, lightweight, low-cost and the possibility of creating large-area devices.[11−14] Nevertheless, the power conversion efficiencies of BHJ solar cells are limited by some drawbacks such as the intrinsic imbalance in the carrier mobility of those conjugated polymer donors due to their relatively high hole mobility but low electron mobility[14] and the lack of suitable *n*-type polymers as electron acceptors.[15] For example, the benchmark BHJ solar cells, P3HT (poly(3-hexylthiophene)):PCBM ([6,6]-phenyl-C61-butyric acid methyl ester), typically show an unimpressive power conversion efficiency of 2−4%.[12,13]

By incorporating fullerene derivatives as electron acceptors for providing an electron transport pathway, the above-mentioned intrinsic imbalance in the carrier mobility of those conjugated polymers can be effectively overcome, causing a power conversion efficiency exceeding 10% for the corresponding polymer BHJ solar cells.[15−17] For instance, a record efficiency (10.6%) was achieved from a tandem polymer BHJ solar cell fabricated using PCBM and ICBA (indene-C_{60} bisadduct fullerene) as the rear cell's and the front cell's electron acceptor, respectively.[16] Except for those commonly used fullerene derivatives, some *n*-type inorganic semiconductor (such as TiO_2, CdSe, ZnO) nanocrystals were also used as electron acceptors in the polymer BHJ (hybrid) solar cells with an impressive power conversion efficiency and high photocurrent,[14] which can be attributed to the efficient dissociation of the photogenerated carriers at the dispersed organic/inorganic interfaces among the domains.[14,17] Theoretically, those separated charge carriers in the BHJ hybrid solar cells can be directly used in a photocatalytic process for H_2 production, just like the dye-sensitized semiconductor system.[18−22] However, there are a few reports on these

Received: March 18, 2015
Revised: May 30, 2015
Published: June 12, 2015

DOI: 10.1021/acssuschemeng.5b00211
ACS Sustainable Chem. Eng. 2015, 3, 1501−1509

polymer-based heterojunction systems applied in the photocatalytic H_2 production.[23−25]

As a new type of polymer catalyst, graphitic carbon nitride (g-C_3N_4) has received much attention due to its visible-light-responsive H_2 production activity and high stability.[26−32] Although the internal quantum yield of Pt/g-C_3N_4 reached up to 26.5% at 400 nm light irradiation,[28] the lack of the absorbance at λ > 460 nm due to its large bandgap (2.7 eV) results in an insufficient sunlight harvesting. As a polymer semiconductor with a suitable bandgap (1.9−2.1 eV) and high hole mobility, P3HT has already been widely used as an electron donor in a BHJ solar cell.[14] Furthermore, a polymer composite of g-C_3N_4 and P3HT (as a sensitizer for the absorption of visible light with longer wavelengths) also resulted in an enhanced H_2 production activity from Na_2S +Na_2SO_3 or TEOA solution as a sacrificial reagent;[23,24] a G-g-C_3N_4-P3HT composite containing graphene (G), g-C_3N_4 and P3HT was used as a photocatalyst to photodegrade methylene blue.[25] Herein, inspired by the concept of polymer-based bulk heterojunction hybrid solar cells, we fabricated a polymer/polymer heterojunction catalyst (P3HT/g-C_3N_4) through a rotary evaporation process of a suspension containing g-C_3N_4 particles (as electron acceptor) and P3HT (electron donor) chloroform solution. Different from the traditional BHJ hybrid solar cells, the loaded P3HT mostly distributed on the particle surfaces of g-C_3N_4 than in bulk to form a surface heterojunction (SHJ) in the present system. Although a very similar heterojunction system has been reported previously as mentioned above, the obtained photoactivity and quantum yield for H_2 production were far from satisfactory from the viewpoint of the practical application.[23,24] To improve further the photoactivity and stability of the obtained SHJ catalyst, the oxidation half-reaction of the photocatalytic H_2 production system is optimized by choosing suitable sacrificial reagents, which has been usually ignored in the previous research.[26−32]

Experimental results indicate that the photocatalytic H_2 production activity of the obtained SHJ catalyst (P3HT/g-C_3N_4) is significantly affected by the types of sacrificial reagents. Among the commonly used ethylenediamine tetraacetic acid (EDTA), triethanolamine (TEOA), ascorbic acid (AA) and Na_2S+Na_2SO_3 solutions, AA as a sacrificial reagent shows the best visible-light-responsive photoactivity, and a H_2 evolution activity up to 3045 μmol/h is attained from the obtained polymer-based SHJ catalyst in a saturated AA solution, which is ~491 times higher than that (6.2 μmol/h) of P3HT/g-C_3N_4 without AA solution under $\lambda \geq$ 500 nm light irradiation. Especially, the SHJ catalyst containing 3 wt % P3HT exhibits an extremely high apparent quantum yield (AQY) of 77.4% at 420 nm light irradiation, which is 26.6 times higher than the reported value (2.9%) of the g-C_3N_4/P3HT polymer composite.[23] Moreover, the SHJ catalyst also exhibits a wide visible/near-infrared (NIR) light responsive ability with AQY of 59.4%, 20.2%, 3.2% and 0.68% at 500, 600, 700 and 800 nm monochromatic light irradiation, respectively. The extremely high photoactivity of the present SHJ catalyst is attributed to the wide visible-light absorption, efficient charge transfer at the interface of P3HT/g-C_3N_4 and suitable oxidation half-reaction caused by the added AA as a sacrificial reagent, which is confirmed by photoluminescence (PL) and time-resolved photoluminescence spectra (TRPS).

EXPERIMENTAL SECTION

SHJ Catalyst Fabrication. The regioregular P3HT was purchased from Sigma-Aldrich and used without further treatment. g-C_3N_4 and its Pt-loaded product (Pt/g-C_3N_4) were prepared by the same method reported in our previous work,[2] and Pt-loaded P3HT (Pt/P3HT) was fabricated according to the previous literature.[23] The polymer/polymer SHJ catalyst (P3HT/g-C_3N_4) was fabricated at room temperature. Typically, Pt/g-C_3N_4 (0.1 g) was mixed with P3HT chloroform solution (1.0 g/L, 3.0 mL), and the resultant suspension was evaporated using rotary evaporation after stirring for 12 h, and the obtained solid was dispersed in ethanol and treated with ultrasonication, and then filtrated through a 0.45 μm nylon filter. After drying at room temperature, the P3HT/g-C_3N_4 catalyst was obtained.

Catalyst Characterization. UV−vis diffuse reflectance absorption spectroscopy (DRS) spectra were obtained with a Shimadzu UV-3600 UV−vis-NIR spectrophotometer that was equipped with an integrating sphere. The crystal phases of the samples were analyzed by using a Bruker D8-Advance X-ray diffractometer (XRD) with Cu Kα radiation (λ = 0.154 178 nm) at 40 kV and 40 mA. X-ray photoelectron spectroscopy (XPS) was measured on a Thermo Fisher ESCALAB 250Xi X-ray photoelectron spectroscope equipped with Al Kα radiation operated at 200 W. Liquid N_2 adsorption−desorption measurements were performed on a Micrometrics ASAP 2020 at 77 K after the sample was degassed at 60 °C. The morphology of the sample was investigated by using a JSM-6700F field emission scanning electron microscopy (FESEM) instrument. The high resolution transmission electron microscopy (HRTEM) observation was conducted on a LaB6 JEM-2100(HR) electron microscope (JEOL Ltd.) working at 200 kV. Photoluminescence (PL) spectra were determined by using a Hitachi Model F-4500 fluorescence spectrophotometer. Time-resolved photoluminescence spectroscopy (TRPS) spectra were obtained on a Model FES 920 system (Edinburgh Instruments) with an excitation wavelength of 377 nm and detection wavelength of 575 nm.

The fluorescence lifetime is calculated according to an exponential fitting equation:

$$\text{fit} = A + B_1 \times e^{-t/\tau_1} + B_1 \times e^{-t/\tau_2} + B_1 \times e^{-t/\tau_3} \quad (1)$$

where A, B_1, B_2 and B_3 are constants and obtained after fitting each decay curve. The statistic values of lifetimes are obtained from 10^5 photons' fluorescence behavior after excitation by computer software. Usually, a more flat tail of the decay curve can give a more accurate and plausible fitted lifetime, and the x-axis (0−1000 ns) only indicates the obtained fluorescence lifetime lies in this time scope.

Photocatalytic H_2 Production Tests. The photocatalytic H_2 production reaction was carried out in a typical photocatalytic system as shown in our previous work.[2] Typically, a photoreaction system (the total volume of the photoreactor is 75 mL, typically with 10 mL of suspension and 65 mL of headspace for gas collection) contains 10 mg of SHJ catalyst and 10 mL of water containing a sacrificial reagent after thorough removal of air before irradiation. A 300 W Xe lamp is used as a light source and a series of cut-off or band-pass filters (such as $\lambda \geq$ 500 nm or λ = 500 ± 10 nm) was equipped to obtain corresponding light regions. The pH value of the system was detected by a FE20/EL20 model pH meter (Mettler-Toledo Instruments Co., Ltd.) and adjusted with NaOH aqueous solution if necessary. The long-term (23 days) photocatalytic tests were conducted: the catalyst was centrifuged and washed with water three times and then dried at 60 °C under vacuum conditions after the last run, and then kept in the dark until the next run by adding new AA aqueous solution. The apparent quantum yield (AQY) was measured and calculated according to the following equation:[6]

$$\text{AQY}\ (\%) = \frac{2 \times \text{number of evolved } H_2 \text{ molecules}}{\text{number of incident photons}} \times 100\% = \frac{2 \times CN_A}{Pt\lambda/hc} \times 100\% \quad (2)$$

DOI: 10.1021/acssuschemeng.5b00211
ACS Sustainable Chem. Eng. 2015, 3, 1501−1509

where C is the H_2 production amount (μmol) per hour; N_A is the Avogadro constant (6.02×10^{23}/mol), h is the Plank constant (6.626×10^{-34} J/s), c is vacuum light velocity (3×10^8 m/s), λ is the monochromatic light wavelength (nm), t is the light irradiation time (1 h) and P is the incident monochromatic light intensity (W), where $P = p \times A$ (see the following).

The incident photons number (N) is obtained by the whole irradiation energy (E) in a given time (t) divided by the energy of one photon (e).[3] Namely, $N = E/e$, where $E = P \times t$, $e = h\nu = hc/\lambda$, and therefore $N = Pt\lambda/hc$. Among which, P is the irradiation flux (W) on the irradiated area and is equal to the product of the irradiation area (A = 11.3 cm^2) and the incident monochromatic light intensity (p, mW/cm^2) detected by a calibrated Si photodiode. Taken the AQY calculation at λ = 420 nm light irradiation as an example, the measured incident monochromatic light intensity is 6.3 mW/cm^2, λ = 420 nm and 1 W = 1 J/s, the AQY can be obtained by using the H_2 production amount at 420 nm light irradiation. For the AQY calculation under $\lambda \geq$ 500 nm with light intensity of 334.8 mW/cm^2, the value is somewhat rough because it is difficult to select a λ for eq 2; therefore, we take 500 nm as the λ for calculation.

RESULTS AND DISCUSSION

The polymer/polymer SHJ catalyst is facilely fabricated by a rotary evaporation process of P3HT chloroform solution containing Pt/g-C_3N_4 (typically, with 1 wt % Pt-loading). UV–vis diffuse reflectance spectra (DRS) shown in Figure 1

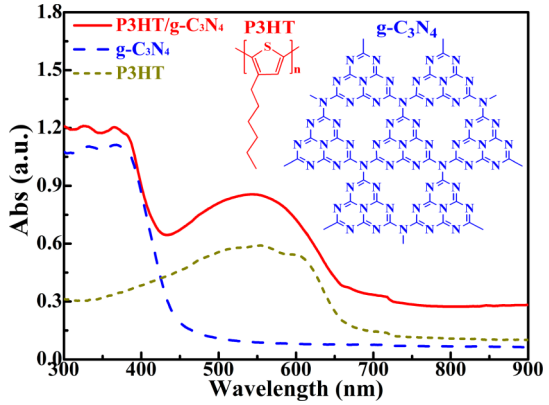

Figure 1. UV–vis diffuse reflectance absorption spectra (DRS) of g-C_3N_4, P3HT and SHJ catalyst (3 wt % P3HT/g-C_3N_4).

exhibit that the onset of the absorption edge of the pristine g-C_3N_4 is at ~450 nm, corresponding to a bandgap of ~2.7 eV, and P3HT absorbs a broad visible-light range (400–700 nm) centered around 550 nm, whereas the polymer/polymer SHJ catalyst (3 wt % P3HT/g-C_3N_4) shows an obvious spectral absorption band in the range of 400–700 nm of P3HT combining with the intrinsic absorption of g-C_3N_4,[26,27] indicating that the SHJ catalyst presents a two-phase composition of g-C_3N_4 and P3HT.

The primary experiments indicate that the photoactivity of the SHJ catalyst (3 wt % P3HT/g-C_3N_4) can be enhanced to different degrees by adding those commonly used sacrificial reagents, such as ethylenediamine tetraacetic acid (EDTA), triethanolamine (TEOA), ascorbic acid (AA), or Na_2S+Na_2SO_3 solution. As can be seen from Figure 2a, AA, TEOA, Na_2S +Na_2SO_3 and EDTA as a sacrificial reagent can give a photocatalytic H_2 production activity of 812, 104, 57 and 44 μmol/h under $\lambda \geq$ 420 nm light irradiation, respectively. Among which, AA solution gives the best photoactivity (812 μmol/h) for H_2 production over 3 wt % P3HT/g-C_3N_4 under $\lambda \geq$ 420 nm light irradiation, which is ~130 times higher than that (6.2 μmol/h) of the 3 wt % P3HT/g-C_3N_4 system without addition of a sacrificial reagent. Although the relative energy levels (Figure 2b) of P3HT and g-C_3N_4 as well as the redox potentials of those sacrificial reagents indicate that each sacrificial reagent used possesses enough thermodynamic electron donating ability to facilitate the regeneration of the excited P3HT after injection electron to the g-C_3N_4,[2,14,23,24,33] it seems that the photoactivity has no clear association with the redox potentials of those sacrificial reagents, and their oxidation processes show more obvious influences on the photoactivity.[34]

The above result on the AA solution gives the best photoactivity for H_2 production over 3 wt % P3HT/g-C_3N_4 among those sacrificial reagents used is very interesting, but the real mechanism of the effect of sacrificial reagent on the H_2 production activity is not clear at this stage. Possibly, AA might provide the most forceful oxidation reaction to facilitate the regeneration of the excited P3HT, thus causing the best photoactivity.[34−37] In general, some organic sacrificial reagents are not only the electron source but also the proton source because they undergo decomposition processes following one electron oxidation and proton(s) production, as shown in Scheme S1 of the Supporting Information.[35] Those possible oxidation processes of the sacrificial reagents are rather complicated, and their oxidation dynamics should be different due to the different pH circumstances, oxidation processes and

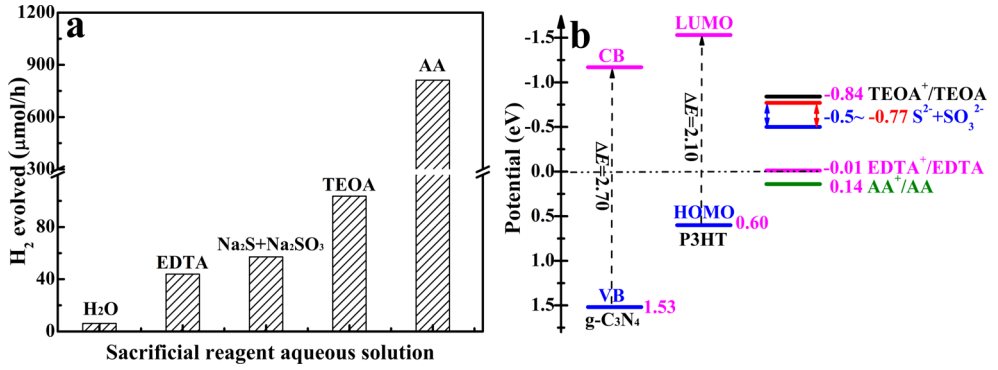

Figure 2. (a) Effects of various sacrificial reagents on the photoactivity of 3 wt % P3HT/g-C_3N_4 under $\lambda \geq$ 420 nm light irradiation. (b) Comparison of the energy levels of P3HT and g-C_3N_4 as well as the redox potentials of those sacrificial reagents used. Conditions: 10 mg of catalyst with 1 wt % Pt-loading, 10 mL of sacrificial reagent solution (0.25 M Na_2S+0.35 M Na_2SO_3; 50 mM AA; 10 mM EDTA; or 10 vol % TEOA) without pH adjusting. Each datum comes from the H_2 production rate in the first 1 h of irradiation.

DOI: 10.1021/acssuschemeng.5b00211
ACS Sustainable Chem. Eng. 2015, 3, 1501−1509

cleavage products.[35−37] Also, the differences in the photoactivity shown in Figure 2a might be due to the different pH values of those sacrificial reagent solutions. Nevertheless, it is reported that a photocatalyst can work better in basic conditions when a basic sacrificial reagent (for example, TEOA) is used, whereas it can also work better in acid conditions when an acid sacrificial reagent (such as EDTA, AA) is used according to the previous reports.[2,4,21,34] Namely, the H_2 production activity usually reaches the highest level when the sacrificial reagent solution's pH value is not adjusted. Although the underlying reason is rarely investigated, some researchers have attributed it to the change of the electron donating ability of the sacrificial reagent when significantly adjusting its pH value.[4,38] Furthermore, it is less likely to get a higher photoactivity of 3 wt % P3HT/g-C_3N_4 through adjusting the other sacrificial reagent solution's pH value because the photoactivity in AA solution is much higher than that in the other sacrificial reagent solutions (Figure 2a).

Because the AA oxidation reaction consumes the photogenerated h^+ of the present SHJ catalyst, its concentration would significantly affect the carrier separation and then the photoactivity. Whereas both of the components in the SHJ catalyst would produce photogenerated h^+ under $\lambda \geq 420$ nm light because the absorption edge of g-C_3N_4 is at ~450 nm and P3HT shows obvious absorption in the range of 400−700 nm (Figure 1). To exclude the influence of the light absorption of g-C_3N_4, $\lambda \geq 500$ nm light irradiation should be beneficial for further investigating the effect of AA on the photoactivity of the present SHJ catalyst. As can be seen from Figure 3, 3 wt % P3HT/g-C_3N_4 shows a photoactivity (838 μmol/h) in the presence of 50 mM AA solution, much higher than that (~12 μmol/h) of 1 wt % Pt/g-C_3N_4 under $\lambda \geq 500$ nm light irradiation. Moreover, 1 wt % Pt/P3HT only shows a very limited H_2 production activity (~1.5 μmol/h) under $\lambda \geq 500$ nm light irradiation. The above results indicate that g-C_3N_4, as an electron acceptor, is necessary in the present SHJ catalyst, and the photoactivity under $\lambda \geq 500$ nm light is mainly contributed by the light absorption of P3HT and its electron transfer toward g-C_3N_4. Nevertheless, 1 wt % Pt/g-C_3N_4 also gives a H_2 production activity of ~12 μmol/h under $\lambda \geq 500$ nm light irradiation, which might be possibly ascribed to the defects existing in the g-C_3N_4.

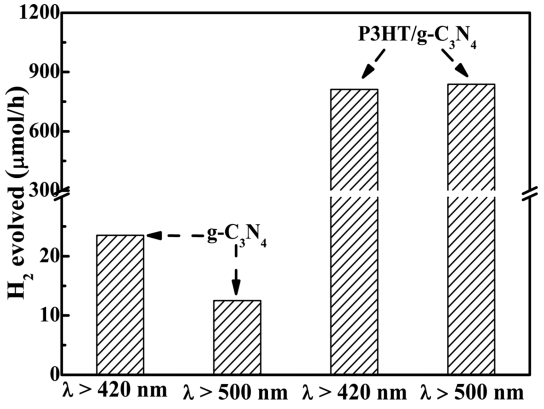

Figure 3. Comparison of the photoactivity of g-C_3N_4 and 3 wt % P3HT/g-C_3N_4 in 50 mM AA solution under different visible-light irradiation. Conditions: 10 mg catalyst with 1 wt % Pt-loading, without pH adjusting. Each datum comes from the H_2 production rates in the first 1 h of irradiation.

Figure 4a shows the effect of AA concentration on the photoactivity and stability for H_2 production over 3 wt % P3HT/g-C_3N_4 under $\lambda \geq 500$ nm light irradiation. After 50 mM AA solution was added, 3 wt % P3HT/g-C_3N_4 showed a photoactivity of 838 μmol/h, which was dramatically enhanced to 2870 μmol/h with further increasing the AA concentration to 250 mM. After that, the photoactivity maintains almost unchanged with slight fluctuation until to a saturated AA solution (~1.70 M), which gives the highest H_2 production activity (3045 μmol/h). It is ~491 times higher than that (6.2 μmol/h) of P3HT/g-C_3N_4 without addition of AA solution. The above results imply that when AA concentration reaches a suitable level, the AA oxidation reaction can support the H_2 production to the most extent, and further enhancing the AA amount would improve the stability for H_2 production. This conjecture can be validated by the effects of AA concentration on the photoactivity and stability for H_2 production over 3 wt % P3HT/g-C_3N_4, as shown in Figure 4b. The H_2 production amount (μmol per 0.5 h) during the three intervals in the presence of 50 mM AA solution decreases tremendously, whereas the decreasing trends can be significantly retarded when AA concentration reaches to 1.0 M or higher, indicating a higher AA concentration would improve the stability for H_2 production over the present SHJ catalyst.

In addition to the AA concentration, the effects of the other photoreaction conditions (such as P3HT amount, catalyst amount, Pt-loading and pH value) on the photoactivity of the SHJ catalyst are also determined and shown in Figure S1 of the Supporting Information. For example, the photoactivity of P3HT/g-C_3N_4 can be improved with enhancing the P3HT amount, and achieves a maximum (2870 μmol/h) at 3 wt % P3HT (Figure S1a of the Supporting Information). The decrease in the photoactivity of P3HT/g-C_3N_4 with higher P3HT content can be ascribed to the agglomeration of the polymer composites due to the P3HT's hydrophobicity, which causes its floating on the solution surface and lowering the light absorption.[23] In addition, the surface active sites (Pt nanoparticles) for H_2 evolution on g-C_3N_4 are possibly blocked by the excessive P3HT, and then causing the decrease in the photoactivity. Moreover, the present SHJ photocatalytic system also exhibits an optimal Pt-loading level and catalyst dosage for H_2 production (Figure S1b,c of the Supporting Information), and the photoactivity shows more sensitive to the pH value of the AA solution (Figure S1d of the Supporting Information), which should be related to the change in the electron donating ability of AA and its oxidation reaction under different pH values as mentioned above.[38] On the basis of the experimental data shown in Figure S1 of the Supporting Information, optimal photoreaction conditions for 3 wt % P3HT/g-C_3N_4 should be 10 mg of catalyst with 1 wt % Pt-loading dispersed in 10 mL of AA solution (250−1700 mM) without pH adjusting.

As mentioned above, the photoactivity can be dramatically enhanced when the AA concentration is enhanced from 0 to 250 mM (Figure 4a), but the stability for H_2 production can be improved only when the AA concentration is >1000 mM (Figure 4b). Figure 5 shows the SHJ catalyst in a saturated AA solution has robust photoactivity even after 23 days of photoreaction under $\lambda \geq 500$ nm light irradiation though there is ~30% activity loss as compared with the first run of the first day. Especially, the biggest activity loss (16.2%) happens in the second run of the first day. It may be partially caused by the accumulation of AA's cleavage products during the photocatalytic procedure and the corresponding products, which

DOI: 10.1021/acssuschemeng.5b00211
ACS Sustainable Chem. Eng. 2015, 3, 1501−1509

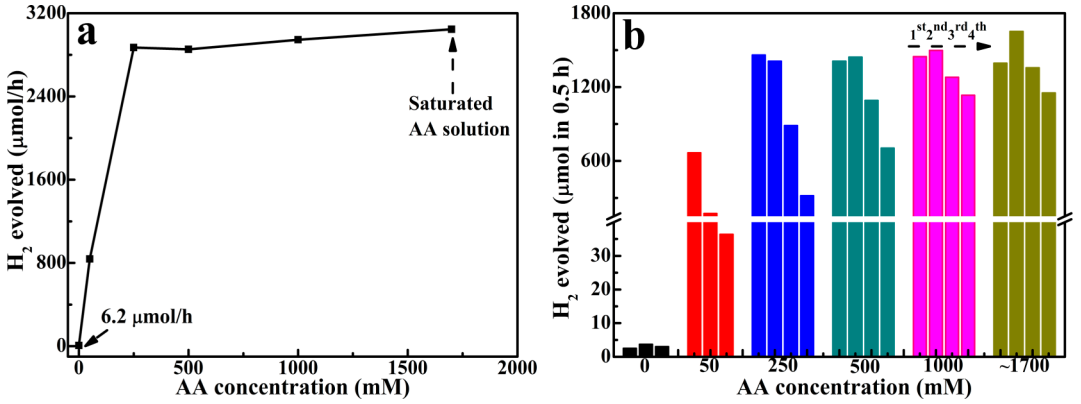

Figure 4. Effects of AA concentration on the photoactivity (a) and stability (b) for H_2 production over 3 wt % P3HT/g-C_3N_4 under $\lambda \geq 500$ nm light irradiation. Conditions: 10 mg of catalyst with 1 wt % Pt-loading, without pH adjusting. Each datum comes from the H_2 production rates in the first 1 h of irradiation.

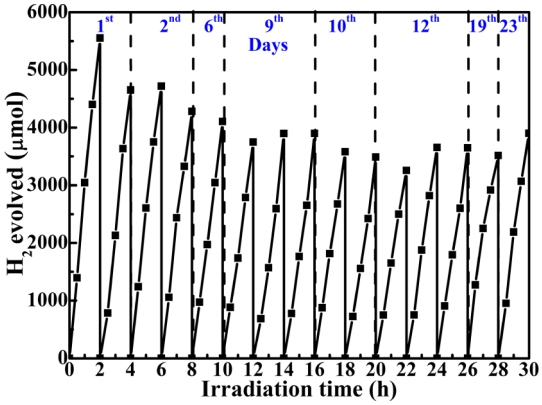

Figure 5. Long-term activity and stability of the SHJ catalyst in the saturated AA solution without pH adjusting. Conditions: 10 mg of catalyst with 1 wt %Pt-loading, 3 wt % P3HT, $\lambda \geq 500$ nm light irradiation.

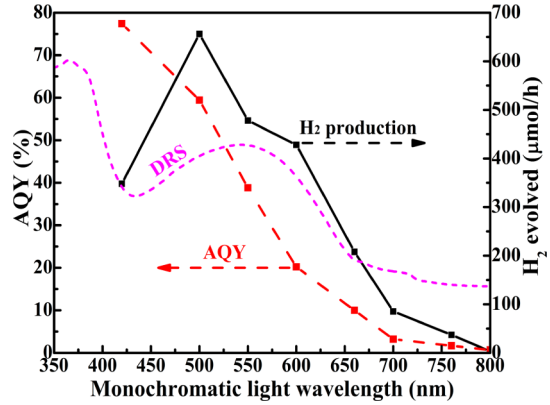

Figure 6. Wavelength-dependent photoactivity and AQY curve of 3 wt % P3HT/g-C_3N_4 in 250 mM AA solution. Conditions: 10 mg of catalyst with 1 wt % Pt-loading.

would be harmful to the light absorption and H_2 production active sites. The color change of the remaining AA solution from colorless to red/brown after the first run is in accordance with their absorption spectra shown in Figure S2 of the Supporting Information, and should be caused by the AA oxidation combining with the regeneration of the oxidized P3HT because the same color change of AA in the air is also observed. Moreover, the activity decrease may also be caused by the SHJ catalyst's photocorrosion, which usually occurs in S-containing materials as reported previously.[23] Furthermore, some nonuniform polymerization or other intrinsic defect existing in the commercial P3HT may also contribute the above activity loss because no huge activity loss happens after the second day's photoreaction. On the whole, 3 wt % P3HT/g-C_3N_4 in a saturated AA solution shows the highest photoactivity up to ~3045 μmol/h under $\lambda \geq 500$ nm light irradiation, and ~70% activity for H_2 production remains even after 23 days of cycle utilization.

The corresponding photoactivity and apparent quantum yield (AQY) values for H_2 production over the present SHJ catalyst under different monochromatic lights are shown in Figure 6. The AQY curve of 3 wt % P3HT/g-C_3N_4 is very similar to the DRS spectrum (Figure 1), indicating that the photoactivity should be dominated by the light absorption of P3HT, producing excitons that further migrate to the P3HT/g-C_3N_4 interfaces. Especially, the present SHJ catalyst with 3 wt % P3HT shows high activity and AQY exceeding 10% in the nearly whole visible-light region (400−660 nm) in addition to a good red/NIR light-responsive ability with an AQY of 3.2% and 0.68% under 700 and 800 nm light irradiation, respectively. This red/NIR light-responsive AQY values are much higher than that of the recently reported metal phthalocyanine dyes.[2,32] Moreover, the AQY values is up to 77.4% and 59.4% at 420 and 500 nm monochromatic light, respectively. The AQY of 77.4% at 420 nm is 26.6 times higher than that (2.9%) of the reported polymer P3HT/g-C_3N_4 composite in Na_2S+Na_2SO_3 solution,[23] and should be a record value in the field of polymer-based catalyst as shown in Table 1, to the best of our knowledge. The higher H_2 production activity of the present SHJ catalyst, as compared to the reported similar P3HT/g-C_3N_4 catalyst,[23,24] is seemingly caused by the different morphology, specific area, microstructure and physicochemical property of g-C_3N_4 obtained by different precursors, different polymerization degrees and regularities of P3HT as well as the selection of a more suitable sacrificial reagent as mentioned above.

The present SHJ catalyst exhibits H_2 production activity (6.2 μmol/h) even without a sacrificial reagent, as shown in Figure 2a, and it seems to indicate the possible overall water splitting in the present SHJ photocatalytic system. However, no obvious O_2 was detected in the present photoreaction system without a sacrificial reagent. It is well know that the O_2 evolution from water oxidation is a 4-electron process, which is much more

DOI: 10.1021/acssuschemeng.5b00211
ACS Sustainable Chem. Eng. 2015, 3, 1501−1509

Table 1. Comparison of the H_2 Production Activity and AQY Value of Various g-C_3N_4-based Catalysts Reported Previously

photocatalyst	Pt [wt %]	reaction volume	sacrificial reagent	HER	AQY [%]	ref
g-C_3N_4 (urea)	3.0	0.02 g of catalyst in 230 mL	TEOA	3327 μmol/hg ($\lambda \geq 395$ nm)	26.5 (λ = 400 nm)	28
EY-g-C_3N_4 (urea)	7.0	0.1 g of catalyst in 80 mL	TEOA	325 μmol in 2 h	18.8 (λ = 400−700 nm)	29
ErB-g-C_3N_4 (urea)	1.25	0.5 g of catalyst in 100 mL	TEOA	652.5 μmol/h ($\lambda \geq 420$ nm)	33.4 (λ = 460 nm) 12.3 (λ = 550 nm)	30
EY-mpg-C_3N_4 (urea)	1.0	0.03 g of catalyst in 80 mL	TEOA	115.5 μmol/h ($\lambda \geq 420$ nm)	24.0 ($\lambda \geq 420$ nm) 8.8 ($\lambda \geq 460$ nm) 1.1 ($\lambda \geq 550$ nm) 19.4 (λ = 550 nm)	31
MgPc-mpg-C_3N_4 (cyanamide)	3.0	0.1 g of catalyst in 100 mL	TEOA	50 μmol/h ($\lambda \geq 420$ nm)	~5.6 (λ = 420 nm) 0.07 (λ = 660 nm)	32
Zn-*tri*-PcNc/g-C_3N_4 (urea)	0.5	0.01 g of catalyst in 10 mL	AA	125.2 μmol/h ($\lambda \geq 500$ nm) 48 μmol/h (λ = 700 nm)	1.85 (λ = 700 nm)	2
P3HT-*g*-C_3N_4 (melamine)	1.0	0.3 g of catalyst in 600 mL	S^{2-}+SO_3^{2-}	560 μmol/h ($\lambda \geq 400$ nm)	2.9 (λ = 420 nm)	23
g-C_3N_4/Au/P3HT/Pt		200 mL	TEOA	320 μmol/h ($\lambda \geq 420$ nm)		24
P3HT-*g*-C_3N_4 (urea)	0.5−1.0	0.01 g of catalyst in 10 mL	S^{2-}+SO_3^{2-} AA	57 μmol/h ($\lambda \geq 420$ nm) 3045 μmol/h ($\lambda \geq 500$ nm)	4.2 (λ = 420 nm) 10.7 ($\lambda \geq 500$ nm) 77.4 (λ = 420 nm) 59.4 (λ = 500 nm) 38.8 (λ = 550 nm) 20.2 (λ = 600 nm) 3.2 (λ = 700 nm) 0.68 (λ = 800 nm)	this work

difficult than the H_2 production from water splitting. Because there are a few H_2 amounts produced from the present SHJ photoreaction system without a sacrificial reagent, the corresponding holes used to the water oxidation for O_2 production are very limited, or may be trapped at the surface or bulk of the present catalyst. By the way, no cocatalyst for O_2 evolution in the present catalyst might also be unfavorable for the O_2 production. Namely, the negligible activity of the present P3HT/g-C_3N_4 in pure water is reasonable because the overall water splitting is a tough reaction, and the photocatalytic reduction half-reaction for H_2 production can be promoted by adding a sacrificial reagent, as can be seen from Figure 2a. Because the present SHJ catalyst exhibits a very limited H_2 production activity (6.2 μmol/h) without a sacrificial reagent, and the total H_2 production amount (~0.81 mmol) is much larger than the added amount (0.5 mmol) of AA solution. It thus can be concluded that the proton source for the evolved H_2 in the present system may mainly stem from the AA oxidation processes, which probably is not in accordance with the procedure shown in Scheme S1 of the Supporting Information.

The above conjecture can be further validated by the changes in the UV−vis absorption (Figure S3 of the Supporting Information) and ESI-MS (Figure S4 of the Supporting Information) spectra as well as the pH value of 250 mM AA aqueous solutions after 1 h of photoreaction containing the SHJ catalyst. Because the H_2 production amount is related to the oxidation half-reaction in the present SHJ photoreaction system, the H^+ reactions with the electrons for H_2 production are significantly influenced by the sacrificial reagent's type and concentration. It is found that the pH value of 250 mM AA aqueous solution (diluted by 10 times) containing the SHJ catalyst increases from 1.73 to 2.13 after 1 h of photoreaction, and their UV−vis absorption spectra (Figure S3 of the Supporting Information) also exhibit that ~15% AA can remain in the solution (diluted by 10^4 times) though ~3 mmol H_2 is evolved for the present system, which exceeds the added AA amount. Moreover, the oxidation processes of AA as sacrificial reagent by the photogenerated h^+ are complicated, and it is difficult to confirm the concrete decomposition process, which might involve multielectron transfer process. Some clues on the oxidation process of AA can be obtained from ESI-MS spectra (Figure S4 of the Supporting Information) of 250 mM AA solution containing the SHJ catalyst before and after 1 h of photoreaction. As can be seen, the main component of the residual AA solution is still AA (m/z = 175.0, AA−H^+) molecules though ~85% AA is oxidized after the photoreaction. That is, a multistep oxidation process of AA does exist in the present system and no obvious partly oxidation product can be observed. In addition, a new relatively strong peak at m/z = 172.9 (AA−3H^+) can be observed from the solution after the photoreaction, implying the oxidation process of AA probably is not accordance with the procedure shown in Scheme S1 of the Supporting Information, and there are electrons' loosing combining with protons' releasing, which cause each AA molecule providing more than one electrons and protons during the oxidation process in the present system, and then the H_2 production amount higher than the added AA.

According to the above discussion and the previous reports,[2,14,23] a possible reaction mechanism is proposed in Figure 7. The more negative LUMO level of P3HT (typically −1.50 eV)[14,23] than the CB of g-C_3N_4 (typically −1.12 eV)[2,23] is favorable for the P3HT's photogenerated electrons transferring to g-C_3N_4, and then trapped by Pt for H_2 production, and the holes in P3HT can be consumed by AA because its redox potential (0.14 eV)[2] is higher than the P3HT's HOMO level (typically 0.6 eV).[23] P3HT may play the roles of sensitization and heterojunction together: extending the light absorption to visible/NIR regions of g-C_3N_4 and the formation of heterojunction with g-C_3N_4, which are favorable for the charge transfer at the interfaces of P3HT/g-C_3N_4. To further investigate the ultrafast electron transfer from P3HT to g-C_3N_4,

DOI: 10.1021/acssuschemeng.5b00211
ACS Sustainable Chem. Eng. 2015, 3, 1501−1509

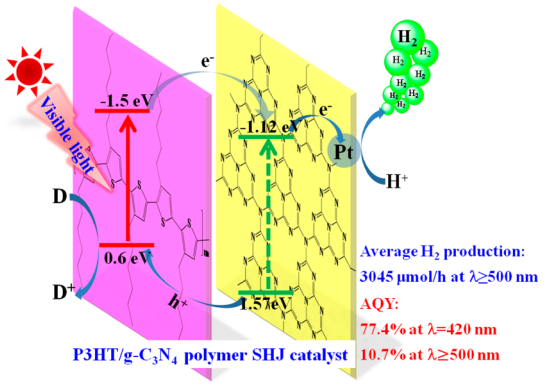

Figure 7. Proposed mechanism of visible-light-driven H_2 production over the SHJ catalyst.

the quenching effect of g-C_3N_4 on the photoluminescence (PL) of P3HT is shown in Figure 8. The strong PL peaks at 576 nm

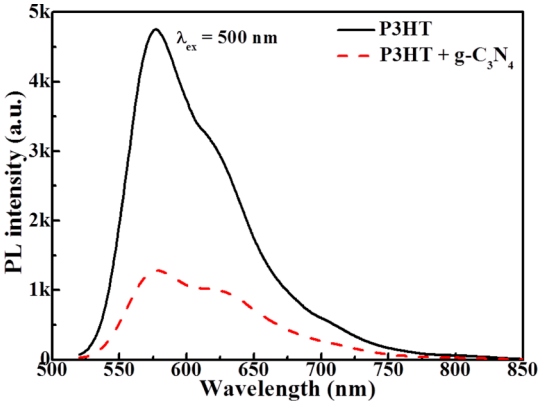

Figure 8. Photoluminescence (PL) spectra of the P3HT chloroform solution and the quenching effect of g-C_3N_4.

related to the fast carrier recombination of P3HT is seriously quenched by g-C_3N_4, implying the efficient charge transfer from P3HT to g-C_3N_4 because there is no overlap between the absorption of g-C_3N_4 and emission of P3HT.[2,23]

Simultaneously, the electron transfer dynamics is investigated by time-resolved photoluminescence spectra (TRPS), as shown in Figure 9, in which the lifetime is a statistic value by observing 10^5 photons' fluorescence behavior after excitation by using an

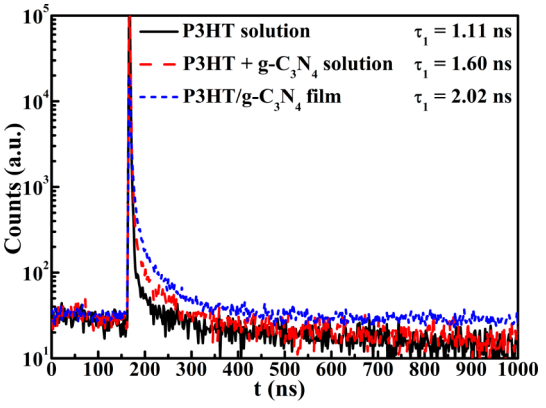

Figure 9. TRPS of P3HT, g-C_3N_4 and P3HT/g-C_3N_4 catalyst suspension or P3HT/g-C_3N_4 film.

excitation wavelength of 377 nm and detection wavelength of 575 nm. The excitation wavelength of 377 nm could also excite g-C_3N_4, but the g-C_3N_4 shows an emission peak at ~453 nm with no emission at 575 nm as reported previously.[23] Also, the selection of detection wavelength (575 nm) is in accordance with the emission of P3HT for investigation of photogenerated electron transfer behavior. The PL lifetime represents the average value of its excited state, and is related to the photogenerated electron transfer and recombination. Usually, a lower recombination rate leads to a longer lifetime. The photogenerated electron transfer to the other material will affect the corresponding excited state lifetime.[40,41] For example, the PL lifetime of Eosin Y (EY) can be prolonged by the electron transfer from the excited EY to graphene (G) or reduced graphene oxide (RGO).[40,41] P3HT gives a PL lifetime of 1.11 ns with quick recombination under excitation, whereas the lifetime is prolonged significantly by either adding g-C_3N_4 to P3HT solution or in the case of the P3HT/g-C_3N_4 film. Similarly, our previous investigation indicated that the PL lifetime of a photosensitizer fixed on a semiconductor film is longer than that in solution though their differences in the lifetime (nanosecond scale) are very limited.[2] This phenomenon is caused by the retarding effect of g-C_3N_4 on the excited P3HT's charge recombination due to electron transfer from P3HT to g-C_3N_4 efficiently.[2] The above PL and TRPS results strongly demonstrate the efficient photogenerated electron transfer from P3HT to g-C_3N_4.[2,39−41]

To examine the morphology, structure and interaction between P3HT and g-C_3N_4 in the SHJ catalyst, the g-C_3N_4 and P3HT/g-C_3N_4 are investigated by the measurements of liquid N_2 adsorption−desorption isotherms, XRD, XPS, SEM and HRTEM. The Brunauer−Emmett−Teller (BET) specific surface area is decreased from 65.6 to 36.0 m^2/g, even after loading 3 wt % P3HT (Figure S5a of the Supporting Information), and the XRD pattern (Figure S5b of the Supporting Information) of the SHJ catalyst exhibits the combination of the characteristic diffraction peaks of both P3HT and g-C_3N_4.[23,42,43] The XPS spectra (Figure S6 of the Supporting Information) of Pt/g-C_3N_4 show the typical binding energy peaks of C, N, O and Pt elements, similar to our previous report,[44,45] and a new binding energy peak ascribe to S 2p can be observed from the SHJ catalyst, indicating the coexisting of the two components of P3HT and g-C_3N_4. Moreover, it can be observed that a slight positive shift in the binding energy for C, N, Pt and a negative shift for O of the Pt/g-C_3N_4 occurred after loading P3HT, implying there are some interactions between P3HT and g-C_3N_4, which can indirectly reflect the formation of heterojunction to some extent. The SEM and TEM images (Figure S7 of the Supporting Information) of g-C_3N_4 and P3HT/g-C_3N_4 show the g-C_3N_4 has a lamellar structure and is almost not affected by the addition of P3HT, even with 20 wt % content, and a HRTEM image clearly shows that some P3HT crystal phases integrate with the amorphous g-C_3N_4. The interplanar spacing of P3HT in SHJ catalyst is ~0.334 nm, close to the lattice distance (0.380 nm) of the possible P3HT's crystal orientations reported previously.[42,43] The above results indicate the formation of a heterojunction between P3HT and g-C_3N_4 in the SHJ catalyst, which would be helpful to the electron transfer through the heterojunction interfaces even though the surface area of catalyst slightly decreases after loading P3HT.

DOI: 10.1021/acssuschemeng.5b00211
ACS Sustainable Chem. Eng. 2015, 3, 1501−1509

CONCLUSIONS

In conclusion, a polymer/polymer surface heterojunction (SHJ) catalyst (P3HT/g-C_3N_4) for wide visible-light-driven H_2 production is successfully constructed by a facile rotary evaporation process. The photocatalytic H_2 production activity of the obtained SHJ catalyst (P3HT/g-C_3N_4) is significantly affected by the types of sacrificial reagents, and ascorbic acid, as a sacrificial reagent, shows the best visible-light-responsive photoactivity among the commonly used ethylenediamine tetraacetic acid, triethanolamine, ascorbic acid and Na_2S +Na_2SO_3 solution. The obtained SHJ catalyst containing 3 wt % P3HT gives a robust photoactivity (3045 μmol/h) for H_2 production in a saturated ascorbic acid solution, which is ~491 times higher than that (6.2 μmol/h) of P3HT/g-C_3N_4 under $\lambda \geq 500$ nm light irradiation. The present results indicate that the importance of a sacrificial reagent cannot be ignored when constructing a photocatalytic H_2 production system, because it actually represents the oxidation half-reaction of the whole photocatalytic reaction and its efficiency will significantly affect the reduction half-reaction for the H_2 production. Moreover, the present SHJ catalyst shows a record apparent quantum yield (77.4%) at 420 nm light irradiation in the field of polymer-based catalyst and wide visible/near-infrared light responsive ability with AQY of 59.4%, 20.2%, 3.2% and 0.68% at 500, 600, 700 and 800 nm monochromatic light irradiation, respectively. The wide light absorption and efficient charge transfer between P3HT and g-C_3N_4 are responsible for the robust photoactivity of the present polymer/polymer SHJ catalyst, demonstrating its promising application in the field of solar energy conversion.

ASSOCIATED CONTENT

Supporting Information

The possible oxidation procedure of various sacrificial reagents, effects of various photoreaction conditions on the H_2 production activity, the comparisons of the UV−vis absorption spectra and mass spectra of AA solution containing the SHJ catalyst before and after the photoreaction, liquid N_2 adsorption−desorption isotherms, XRD patterns, XPS spectra, FESEM and TEM images of the SHJ catalyst. The Supporting Information is available free of charge on the ACS Publications website at DOI: 10.1021/acssuschemeng.5b00211.

AUTHOR INFORMATION

Corresponding Author

*T. Peng. Fax: 86 27 6875 2237. Tel.: 86 27 6875 2237. E-mail: typeng@whu.edu.cn.

Notes

The authors declare no competing financial interest.

ACKNOWLEDGMENTS

The present work is supported by the Natural Science Foundation of China (21271146, 20973128 and 20871096), the Fundamental Research Funds for the Central Universities (2042014kf0228) and the Funds for Creative Research Groups of Hubei Province (2014CFA007), China.

REFERENCES

(1) Wang, H.; Zhang, L.; Chen, Z.; Hu, J.; Li, S.; Wang, Z.; Liu, J.; Wang, X. Semiconductor heterojunction photocatalysts: Design, construction, and photocatalytic performances. *Chem. Soc. Rev.* **2014**, *43*, 5234−5244.

(2) Zhang, X. H.; Yu, L. J.; Zhuang, C. S.; Peng, T. Y.; Li, R. J.; Li, X. G. Highly asymmetric phthalocyanine as a sensitizer of graphitic carbon nitride for extremely efficient photocatalytic H_2 production under near-infrared light. *ACS Catal.* **2014**, *4*, 162−170.

(3) Peng, T. Y.; Zhang, X. H.; Zeng, P.; Li, K.; Zhang, X. G.; Li, X. G. Carbon encapsulation strategy of Ni co-catalyst: Highly efficient and stable Ni@C/CdS nanocomposite photocatalyst for hydrogen production under visible light. *J. Catal.* **2013**, *303*, 156−163.

(4) Zhang, X. H.; Veikko, U.; Mao, J.; Cai, P.; Peng, T. Y. Visible-light-induced photocatalytic hydrogen production over binuclear Ru^{II}-bipyridyl dye-sensitized TiO_2 without noble metal loading. *Chem.—Eur. J.* **2012**, *18*, 12103−12111.

(5) Zhang, X.; Peng, T.; Yu, L.; Li, R.; Li, Q.; Li, Z. Visible/near-infrared-light-induced H_2 production over g-C_3N_4 cosensitized by organic dye and zinc phthalocyanine derivative. *ACS Catal.* **2015**, *5*, 504−510.

(6) Liu, J.; Liu, Y.; Liu, N.; Han, Y.; Zhang, X.; Huang, H.; Lifshitz, Y.; Lee, S.; Zhong, J.; Kang, Z. Metal-free efficient photocatalyst for stable visible water splitting via a two-electron pathway. *Science* **2015**, *347*, 970−974.

(7) Qu, Y.; Duan, X. Progress, challenge and perspective of heterogeneous photocatalysts. *Chem. Soc. Rev.* **2013**, *42*, 2568−2580.

(8) Yang, J.; Wang, D.; Han, H.; Li, C. Roles of cocatalysts in photocatalysis and photoelectrocatalysis. *Acc. Chem. Res.* **2013**, *46*, 1900−1909.

(9) Swierk, J.; Mallouk, T. Design and development of photoanodes for water-splitting dye-sensitized photoelectrochemical cells. *Chem. Soc. Rev.* **2013**, *42*, 2357−2387.

(10) Wu, Y.; Zhu, W. Organic sensitizers from D-π-A to D-A-π-A: Effect of the internal electron-withdrawing units on molecular absorption, energy levels and photovoltaic performances. *Chem. Soc. Rev.* **2013**, *42*, 2039−2058.

(11) Huang, Y.; Kramer, E.; Heeger, A.; Bazan, G. Bulk heterojunction solar cells: Morphology and performance relationships. *Chem. Rev.* **2014**, *114*, 7006−7043.

(12) Dang, M.; Hirsch, L.; Wantz, G.; Wuest, J. Controlling the morphology and performance of bulk heterojunctions in solar cells. Lessons learned from the benchmark poly(3-hexylthiophene):[6,6]-phenyl-C_{61}-butyric acid methyl ester system. *Chem. Rev.* **2013**, *113*, 3734−3765.

(13) Dang, M. T.; Hirsch, L.; Wantz, G. P3HT:PCBM, best seller in polymer photovoltaic research. *Adv. Mater.* **2011**, *23*, 3597−3602.

(14) Zhou, Y.; Eck, M.; Krüger, M. Bulk-heterojunction hybrid solar cells based on colloidal nanocrystals and conjugated polymers. *Energy Environ. Sci.* **2010**, *3*, 1851−1864.

(15) Earmme, T.; Hwang, Y.; Murari, N.; Subramaniyan, S.; Jenekhe, S. All-polymer solar cells with 3.3% efficiency based on naphthalene diimide-selenophene copolymer acceptor. *J. Am. Chem. Soc.* **2013**, *135*, 14960−14963.

(16) You, J.; Dou, L.; Yoshimura, K.; Kato, T.; Ohya, K.; Moriarty, T.; Emery, K.; Chen, C. C.; Gao, J.; Li, G.; Yang, Y. A polymer tandem solar cell with 10.6% power conversion efficiency. *Nat. Commun.* **2013**, *4*, 1446.

(17) He, Z.; Zhong, C.; Su, S.; Xu, M.; Wu, H.; Cao, Y. Enhanced power-conversion efficiency in polymer solar cells using an inverted device structure. *Nat. Photonics* **2012**, *6*, 591−595.

(18) Wen, F.; Li, C. Hybrid artificial photosynthetic systems comprising semiconductors as light harvesters and biomimetic complexes as molecular cocatalysts. *Acc. Chem. Res.* **2013**, *46*, 2355−2364.

(19) Chen, X.; Shen, S.; Guo, L.; Mao, S. Semiconductor-based photocatalytic hydrogen heneration. *Chem. Rev.* **2010**, *110*, 6503−6570.

(20) Osterloh, F. Inorganic nanostructures for photoelectrochemical and photocatalytic water splitting. *Chem. Soc. Rev.* **2013**, *42*, 2294−2320.

(21) Zhang, X. H.; Yu, L. J.; Zhuang, C. S.; Peng, T. Y.; Li, R. J.; Li, X. G. Highly efficient visible/near-IR-light-driven photocatalytic H_2

DOI: 10.1021/acssuschemeng.5b00211
ACS Sustainable Chem. Eng. 2015, 3, 1501−1509

production over asymmetric phthalocyanine-sensitized TiO_2. *RSC Adv.* **2013**, *3*, 14363−14370.
(22) Yu, L. J.; Zhang, X. H.; Zhuang, C. S.; Lin, L.; Li, R. J.; Peng, T. Y. Syntheses of asymmetric zinc phthalocyanines as sensitizer of Pt-loaded graphitic carbon nitride for efficient visible/near-IR-light-driven H_2 production. *Phys. Chem. Chem. Phys.* **2014**, *16*, 4106−4114.
(23) Yan, H.; Huang, Y. Polymer composites of carbon nitride and poly(3-hexylthiophene) to achieve enhanced hydrogen production from water under visible light. *Chem. Commun.* **2011**, *47*, 4168−4170.
(24) Zhang, Y.; Mao, F.; Yan, H.; Liu, K.; Cao, H.; Wu, J.; Xiao, D. A polymer-metal- polymer-metal heterostructure for enhanced photocatalytic hydrogen production. *J. Mater. Chem. A* **2015**, *3*, 109−115.
(25) Gawanda, S.; Thakare, S. Ternary polymer composite of graphene, carbon nitride, and poly(3-hexylthiophene): An efficient photocatalyst. *ChemCatChem* **2012**, *4*, 1759−1763.
(26) Wang, X.; Maeda, K.; Thomas, A.; Takanabe, K.; Xin, G.; Carlsson, J.; Gomen, K.; Antonietti, M. A metal-free polymeric photocatalyst for hydrogen production from water under visible light. *Nat. Mater.* **2009**, *8*, 76−80.
(27) Martin, D.; Reardon, P.; Moniz, S.; Tang, J. Visible light-driven pure water splitting by a nature-inspired organic semiconductor-based system. *J. Am. Chem. Soc.* **2014**, *136*, 12568−12571.
(28) Martin, D.; Qiu, K.; Shevlin, S.; Handoko, A.; Chen, X.; Guo, Z.; Tang, J. Highly efficient photocatalytic H_2 evolution from water using visible light and structure-controlled graphitic carbon nitride. *Angew. Chem., Int. Ed.* **2014**, *53*, 9240−9245.
(29) Xu, J.; Li, Y.; Peng, S.; Lu, G.; Li, S. Eosin Y-sensitized graphitic carbon nitride fabricated by heating urea for visible light photocatalytic hydrogen evolution: The effect of the pyrolysis temperature of urea. *Phys. Chem. Chem. Phys.* **2013**, *15*, 7657−7665.
(30) Wang, Y.; Hong, J.; Zhang, W.; Xu, R. Carbon nitride nanosheets for photocatalytic hydrogen evolution: Remarkably enhanced activity by dye sensitization. *Catal. Sci. Technol.* **2013**, *3*, 1703−1711.
(31) Min, S.; Lu, G. Enhanced electron transfer from the excited eosin Y to mpg-C_3N_4 for highly efficient hydrogen evolution under 550 nm irradiation. *J. Phys. Chem. C* **2012**, *116*, 19644−19652.
(32) Takanabe, K.; Kamata, K.; Wang, X.; Antonietti, M.; Kubota, J.; Domen, K. Photocatalytic hydrogen evolution on dye-sensitized mesoporous carbon nitride photocatalyst with magnesium phthalocyanine. *Phys. Chem. Chem. Phys.* **2010**, *12*, 13020−13025.
(33) Bessekhouad, Y.; Trari, M. Photocatalytic hydrogen production fromsuspension of spinel powders AMn_2O_4 (A = Cu and Zn). *Int. J. Hydrogen Energy* **2002**, *27*, 357−362.
(34) Choi, S.; Yang, H.; Kim, J.; Park, H. Organic dye-sensitized TiO_2 as a versatile photocatalyst for solar hydrogen and environmental remediation. *Appl. Catal., B* **2012**, *121/122*, 206−213.
(35) Wu, L.; Chen, B.; Li, Z.; Tung, C. Enhancement of the efficiency of photocatalytic reduction of protons to hydrogen via molecular assembly. *Acc. Chem. Res.* **2014**, *47*, 2177−2185.
(36) Chai, B.; Peng, T. Y.; Zeng, P.; Zhang, X. H.; Liu, X. G. Template-free hydrothermal synthesis of $ZnIn_2S_4$ floriated microsphere as an efficient photocatalyst for H_2 production under visible-light irradiation. *J. Phys. Chem. C* **2011**, *115*, 6149−6155.
(37) Esswein, A.; Nocera, D. Hydrogen production by molecular photocatalysis. *Chem. Rev.* **2007**, *107*, 4022−4047.
(38) Han, Z.; Qiu, F.; Eisenberg, R.; Holland, P.; Krauss, T. Robust photogeneration of H_2 in water using semiconductor nanocrystals and a nickel catalyst. *Science* **2012**, *338*, 1321−1324.
(39) Zhu, M.; Li, Z.; Xiao, B.; Lu, Y.; Du, Y.; Yang, P.; Wang, X. Surfactant assistance in improvement of photocatalytic hydrogen production with the porphyrin noncovalently functionalized graphene nanocomposite. *ACS Appl. Mater. Interfaces* **2013**, *5*, 1732−1740.
(40) Kong, C.; Min, S.; Lu, G. Dye-sensitized NiS_x catalyst decorated on graphene for highly efficient reduction of water to hydrogen under visible light irradiation. *ACS Catal.* **2014**, *4*, 2763−2769.
(41) Min, S.; Lu, G. Sites for high efficient photocatalytic hydrogen evolution on a limited-layered MoS_2 cocatalyst confined on graphene sheets-the role of graphene. *J. Phys. Chem. C* **2012**, *116*, 25415−25424.
(42) Erb, T.; Zhokhavets, U.; Gobsch, G.; Raleva, S.; Stühn, B.; Schilinsky, P.; Waldauf, C.; Brabec, C. J. Correlation between structural optical properties of composite polymer/fullerene films for organic solar cells. *Adv. Funct. Mater.* **2005**, *15*, 1193−1196.
(43) Ma, W.; Yang, C.; Gong, X.; Lee, K.; Heeger, A. Thermally stable, efficient polymer solar cells with nanoscale control of the interpenetrating network morphology. *Adv. Funct. Mater.* **2005**, *15*, 1617−1622.
(44) Mao, J.; Peng, T. Y.; Zhang, X. H.; Li, K.; Ye, L. Q.; Zan, L. Effect of graphitic carbon nitride microstructures on the activity and selectivity of photocatalytic CO_2 reduction under visible light. *Catal. Sci. Technol.* **2013**, *3*, 1253−1260.
(45) Chai, B.; Peng, T. Y.; Mao, J.; Li, K.; Zan, L. Graphitic carbon nitride (g-C_3N_4)-Pt-TiO_2 nanocomposite as an efficient photocatalyst for hydrogen production under visible light irradiation. *Phys. Chem. Chem. Phys.* **2012**, *14*, 16745−16752.

DOI: 10.1021/acssuschemeng.5b00211
ACS Sustainable Chem. Eng. 2015, 3, 1501−1509